Journal of Materials Chemistry C

Accepted Manuscript

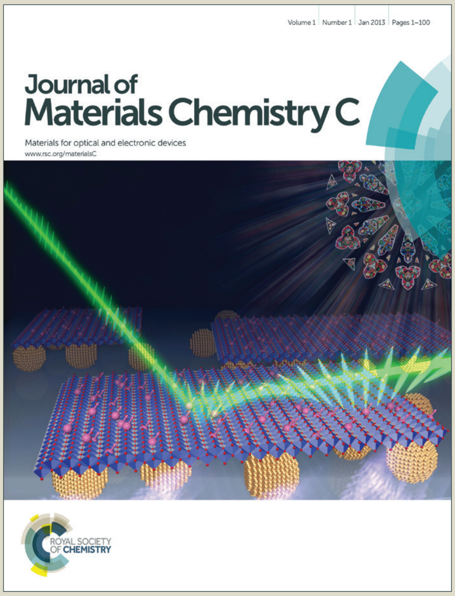

ROYAL SOCIETY OF CHEMISTRY

www.rsc.org/materialsC

Superior characteristics of graphene field effect transistor enclosed by chemical-vapor-deposition-grown hexagonal boron nitride

Muhammad Waqas Iqbal[1], Muhammad Zahir Iqbal[1], Xiaozhan Jin[2], Jonghwa Eom[1]* and Chanyong Hwang[2]*

[1]Department of Physics and Graphene Research Institute, Sejong University, Seoul 143-747, Korea

[2]Center for Nanometrology, Korea Research Institute of Standards and Science, Daejeon 305-340, Korea

ABSTRACT: We report on the characterization of high-quality chemical-vapor-deposition (CVD)-grown graphene devices on CVD-grown hexagonal boron nitride (h-BN). Electrical transport measurements and Raman spectroscopy showed that the graphene devices on the h-BN film presented superior carrier mobility and suppression of charged impurities. The hole mobility of graphene on h-BN and on h-BN/graphene/h-BN at 4.2 K was 18000 and 20000 cm^2/Vs, respectively. The CVD-grown h-BN provided not only an ideal substrate for graphene but also a protection layer against unwanted doping by O_2. The h-BN/graphene/h-BN sandwich structure offers a great advantage for the manufacture of stable graphene electronic devices.

KEYWORDS: graphene · boron nitride · CVD · electrical transport · mobility · protection

*e-mail: eom@sejong.ac.kr, cyhwang@kriss.re.kr

1. Introduction

Graphene is highly sensitive to its local surroundings[1,2], such as substrate screening and impurities, due to the one-atom-thick nature of the C membrane, where each atom is exposed to the peripheral environment[1]. The electronic mobility of graphene transferred on a Si/SiO$_2$ substrate is far less than the theoretically predicted value. Graphene's electrical properties are strongly affected by the interfacial charged impurities, surface roughness, and surface phonons of the Si/SiO$_2$ substrates[3]. Suspending graphene offers considerable improvements in device quality[4,5]; however, this kind of geometry imposes severe limitations on device fabrication[6,7]. The improvement in sample quality in a substrate-supported geometry is crucial for the future progress of graphene technology[8]. Efforts have been made to develop alternatives to Si/SiO$_2$; however, other oxide substrates have naturally caused similar surface effects and continue to be problematic on the graphene samples. Hexagonal boron nitride (h-BN) is a substrate[9-11], which can be used to eliminate problematic surface effects in graphene samples, as h-BN has a large band gap, is comparatively inert, does not have dangling bonds, possesses low density of charged impurities and is naturally flat[12-17].

There are limitations in obtaining an h-BN film from bulk h-BN crystal by the micromechanical cleavage method[18,19] regarding available sizes and applications to device fabrication[20]. The h-BN flakes exfoliated from h-BN microcrystals are randomly located on the SiO$_2$ substrate, and in the subsequent process graphene should be manually positioned to align with the location of the h-BN film. Although high-quality graphene devices may be achieved on the exfoliated h-BN, it is difficult to maintain uniformity of the device on a wafer scale and to apply the process to mass production with this method[21]. Recently, chemical vapor deposition (CVD) has been used as an approach for growing large-area h-BN films[22-24]. Here, we show uniform and continuous h-BN films synthesized on a large area by using the chemical vapor deposition (CVD) method and a simplified transfer technique to avoid residue between graphene and the h-BN interface. Using the traditional transfer method of graphene and h-BN, there is a higher probability of having polymethyl methacrylate (PMMA) and other residue between the graphene and the h-BN interface[25]. We have focused to make a clean interface between graphene and h-BN. We also present transport and Raman measurement on large area h-BN/G/h-BN devices with high performance. The direct growth of graphene on h-BN is an alternative for avoiding the formation of residue between the graphene and the h-BN interface[26-28], but the quality of graphene so far is not as good as the graphene grown directly on Cu foil. We present that highly performed, large scale, stable devices can be fabricated using CVD-grown graphene and CVD-grown h-BN.

2. Experimental

2.1. Device fabrication and characterization

We fabricated graphene/h-BN devices using photolithography, e-beam lithography, and O_2 plasma etching. Large electrode patterns with Cr/Au (6/30 nm) film were deposited using a thermal evaporator after standard photolithography. To characterize h-BN/graphene/h-BN an additional layer of h-BN was transferred on graphene/h-BN after pattern the electrodes. The characteristics of the single-layer graphene and h-BN film were examined with optical microscopy and Raman spectroscopy. Raman mapping was also used to examine CVD-grown graphene transferred on an h-BN film sheet at room temperature. The laser wavelength of the Raman microspectrometer was 514 nm, and the power was kept below 1.0 mW to avoid laser-induced heating. The laser spot size of Raman spectroscopy was 0.7 μm for the wavelength of 514 nm. The step size is 2 μm and scanning area is 20×20 μm^2. The Dirac point of each graphene device was measured by the gate-voltage-dependent resistivity measurement using the four-probe configuration with lock-in amplifier in vacuum at different temperatures. After device fabrication was completed, all devices were annealed in a tube furnace at a temperature of 200 °C in a flow of Ar/H_2 gas for 2 hours. To characterize h-BN as a layer providing protection from oxidation of graphene, we investigated the deep ultraviolet light (DUV) effect under O_2 gas flow for CVD-grown graphene on Si/SiO_2, h-BN, and h-BN/graphene/h-BN by Raman spectroscopy and transport measurement. Electrical transport measurement was also performed for our devices after exposure to deep ultraviolet light (DUV) with a dominant wavelength of $\lambda = 220$ nm and average intensity of 11 mW/cm^2 in O_2 gas flow for a certain time. The device was placed in quartz tube, and glass quartz was pumped to evacuate air. Then O_2 gas was introduced in quartz tube with continuous flow. Then, DUV light was turned on to shine on the device in the quartz tube[29].

2.2. Growth and transfer method

The h-BN film was grown on 25-μm-thick high-purity (99.8%) Cu foils by using thermal chemical vapor deposition (CVD) as shown in the schematic diagram in Figure 1a (for growth detail, see the Methods section). We have used atomic force microscopy (AFM) to confirm the thickness and morphology of CVD-grown h-BN sample as shown in the Supporting Information. The thickness measured by AFM is ~ 4.3 nm, which indicates 6 layers of CVD-grown h-BN. However, the CVD-grown h-BN film was too fragile to be transferred onto the Si substrate by the normal transfer method for CVD-grown graphene.[30] To overcome this problem, we used a combined transfer method as outlined in Figure S1a. First, the PMMA was spin-coated on the CVD-grown graphene film on Cu foil. Next, the Cu foil was etched out by soaking in an ammonium persulfate (APS) solution for 24 h. The graphene film on PMMA was transferred onto the as-grown h-BN film on a Cu foil, which was also etched out by APS solution. Finally, the h-BN/graphene/PMMA film was transferred onto a Si substrate. After the PMMA film was removed by soaking in acetone, CVD-grown graphene on CVD-grown h-BN film was obtained on the Si substrate with a 300-nm-thick SiO_2 capping layer.

3. Results and discussion

The detailed growth morphology was examined by scanning electron microscope (SEM) (see Figure 1b, c). The typical grain size of h-BN grown on Cu foil is about 5 - 10 μm in this experiment. Figure 1b shows the size and shape of the h-BN island at the initial growth. The triangular shaped film in the initial growth stage is typically observed because the nitrogen terminated structure is more energetically stable. The coalescence behavior is quite interesting considering the immobile nature of the islands. Once the islands start to nucleate at some points, they are not easily movable. However, the island shape remains triangular all the time before the coalescence. The remaining blank area is filled to make a continuous film at the final stage as seen in Figure 1c. In the optical micrograph of the CVD-grown graphene device used in our study (Figure 1d), one part of the graphene was on the Si/SiO_2 substrate and the other part was on the CVD-grown h-BN film. In the Raman spectrum of CVD-grown h-BN transferred on the Si/SiO_2 substrate (Figure 1e), the h-BN peak was observed at 1369 cm^{-1}, which confirms the growth and clean transfer of the h-BN film from Cu foil.[31]

3.1. Raman Spectra measurement on different substrates

We examined graphene on three different types of substrates. The first was on SiO_2 film, the second was on CVD-grown h-BN film, and the last graphene layer was sandwiched between h-BN films, which were fabricated by transferring an additional layer of h-BN film on top of the graphene on the h-BN film. The Raman spectra of CVD-grown graphene on SiO_2 film, h-BN film, and the graphene sandwich between CVD-grown h-BN films are shown in Figure 2a. G and 2D peaks were observed at 1581.5 and 2688.6 cm^{-1} on the h-BN film, whereas the G and 2D peaks were located at 1584.6 and 2684.1 cm^{-1} on the SiO_2 film. The peak at 1369 cm^{-1} of the graphene on h-BN film was attributed to the h-BN peak (see inset of Figure 2a. [31] It is critical to distinguish between the h-BN peak and the defect-induced D peak appearing around 1345 cm^{-1} in the Raman spectrum of graphene.[32] To distinguish the h-BN peak from the D peak, Raman spectra were recorded at edge regions of the graphene where defects were known to be visible.[33] The inset in Figure 2a represents the corresponding Raman spectrum of graphene on h-BN film at the edge. The Raman spectra recorded at the edge of graphene showed a second peak arising at around 1345 cm^{-1}, which was not observable in the central region and could be clearly distinguished from the h-BN peak at 1369 cm^{-1}. No D peak was observed in regions of graphene away from the edges, in either h-BN or SiO_2 films. The absence of the D peak on both films confirmed the high quality of graphene and was evidence of a clean transfer process.[34,35]

To understand the substrate effect of graphene on SiO_2 film, h-BN film, and graphene sandwiched between h-BN films, respectively, a comparison of the G- and 2D-peak positions and the full-width-at-half-maximum (FWHM) is presented in Figure 2b and c. We observed significant differences in peak position and FWHM. The G peak was observed at 1585.8 cm^{-1} on the SiO_2 film, whereas the G peak on h-BN film was centered at 1581.5 cm^{-1} (Figure 2b). The observation of red-shift in the G-peak position for graphene on h-BN film was reported and attributed to a reduced doping effect.[36] The reduced doping effect was also confirmed by the increase in the FWHM of the G peak in graphene on h-BN film. The FWHM of the G peak was 12.3 cm^{-1} on the SiO$_2$ film and 16.2 cm^{-1} on the h-BN film. The 2D peak was observed at 2684.1 cm^{-1} on the SiO$_2$ film, whereas the 2D peak on the h-BN film was centered at 2688.6 cm^{-1}, as shown in Figure 2c. The change in FWHM of the 2D peak is even more pronounced on h-BN film. While the FWHM of the 2D peak on the SiO$_2$ substrate was 34.1 cm^{-1}, the FWHM of the 2D peak on h-BN film was 24.6 cm^{-1}, which is close to that of suspended graphene.[37] We note that the FWHM of the 2D peak does not depend on doping level. It was reported that Raman measurements of gated graphene on SiO$_2$ film did not show any considerable dependence on the charge carrier density.[38] Hence, the reduced FWHM of the 2D peak on h-BN film should originate from some other effect. A similar reduced FWHM of the 2D peak (~22 cm^{-1}) has also been observed for suspended graphene. The FWHM of the 2D peak for graphene on SiO$_2$ film is increased due to the presence of charge impurities and the substrate roughness[37,39] which cause a smaller lifetime for the excited electronic states during the double-resonant Raman process via enhanced electron scattering.

A G peak of h-BN/graphene/h-BN has been observed at 1581.1 cm^{-1}, which is a similar position to the G peak of graphene on h-BN film, as can be seen in Figure 2b. In contrast to the G-peak position, a 2D-peak position of h-BN/graphene/h-BN has been observed at 2694.2 cm^{-1}, which is considerably blue-shifted compared with the 2D-peak position of graphene on SiO$_2$ film or h-BN film.[40,41]

Figure 3 presents the statistical distribution of the Raman spectra for 50 × 50 μm^2 graphene on different substrates. Normalized frequency represents the normalized occurrence number of the Raman shift in the scanning area. The highest normalized frequency corresponds to the maximum occurrence number of the Raman shift in the scanning area. Figure 3a presents the statistical distribution of the G-peak position of graphene on SiO$_2$ film, h-BN film, and h-BN/graphene/h-BN. The mean value of the G-peak position depended on the substrate, and the h-BN substrate gave the largest red-shift of the G-peak position. The 2D-peak position also showed strong substrate dependence, as shown in Figure 3b. The statistical distribution of the Raman intensity ratio of I_{2D}/I_G for graphene on the SiO_2 film, h-BN film, and h-BN/graphene/h-BN is shown in Figure 3c. The mean value of the I_{2D}/I_G ratio was 2.5 for graphene on the SiO_2 substrate, 5 on the h-BN substrate, and 6.8 on the h-BN/graphene/h-BN structure. Figure 3d shows the statistical distribution of the FWHM of the 2D peak on different substrates.

Uniform quality is an important requirement for mass production. The homogeneity of graphene quality depends on the substrates (Figure 3). The largest standard deviations of the G- and 2D-peak position, I_{2D}/I_G, and FWHM of the 2D peak were found for graphene on the SiO_2 substrate, and the smallest were found on h-BN/graphene/h-BN, indicating that a higher uniformity of graphene quality can be acquired by a sandwich structure between the h-BN films.

3.2. Electrical transport measurement on different substrates at different temperatures

The high quality of graphene can be further confirmed by examining the electronic transport characteristics. Figure 4a shows the back-gate-voltage (V_{bg})-dependent resistivity for CVD-grown graphene on h-BN film at different temperatures. The inset shows an optical micrograph of a graphene Hall bar structure for transport measurement. The resistivity was measured by a four-probe method using lock-in amplifier techniques. The Dirac point of the graphene sample on h-BN film was around $V_{bg} = 0$ V, indicating the undoped characteristics of pristine graphene. Figure 4b presents the longitudinal resistivity (black curve) and the Hall conductance (red curve) as a function of V_{bg} at the magnetic field B = 9 T and at the temperature T = 0.33 K. The Hall plateau at the filling factors $\nu = \pm 2, \pm 6$, and ± 10 indicates that the sample is monolayer graphene.[42-44] In addition, the Hall plateau at the filling factor ν = ±1 was observed at a high magnetic field of 9 T (Figure 4c). It originates from a lift of spin degeneracy, which was reported for the high-quality graphene on h-BN. [11, 30] We further investigated the charge carrier mobility of graphene on different substrates at various temperatures. The hole mobility among graphene devices on different substrates is compared in Figure 4d. The filed effect mobility was obtained by using relation $\mu = (1/C_g)(\partial\sigma/\partial V_g)$, where σ is the conductivity of samples and V_g is the gate voltage. C_g is the gate capacitance of ~115 aF/μm^2 for our Si/SiO_2 substrate.[45,46] The hole mobility of graphene on SiO_2, h-BN, and h-BN/graphene/h-BN was 2800, 6300, and 7400 cm^2/Vs, respectively, at T = 300 K, and 4000, 18000, and 20000 cm^2/Vs, respectively, at T = 4.2 K. For the entire temperature range in this experiment, h-BN/graphene/h-BN showed the highest mobility.

3.3. Electrical transport measurement under DUV light in the presence of oxygen on different substrates

To elucidate the doping effect of graphene on different substrates, electrical transport measurement was performed for graphene samples after exposure to deep ultraviolet light (DUV) with a dominant wavelength of λ = 220 nm and average intensity of 11 mW/cm^2 in O_2 gas flow for a certain time. DUV can provide enough energy for O_2 to be adsorbed on the surface of graphene.[29,46,47] Figure 5a, b, and c shows the gate-voltage-dependent resistivity of graphene on SiO_2, h-BN, and h-BN/graphene/h-BN after DUV exposure in O_2 gas flow (DUV+O_2), respectively. DUV+O_2 treatment was performed after device fabrication was completed. The Dirac point shifts toward a positive gate voltage as DUV illumination time increases, indicating p-type doping for all substrates. However, judging from the Dirac point shift, the doping intensity is not the same for graphene on different substrates, even with the same DUV+O_2 treatment. Figure 5d illustrates the Dirac point shift as a function of DUV+O_2 treatment time for different substrates. The Dirac point of graphene on SiO_2 film was observed at 21, 28, 32, and 36 V after 5, 10, 20, and 30 min of DUV+O_2 treatment, respectively. The Dirac point of graphene on h-BN film was observed at 9.4, 12.7, 15, and 20 V after 5, 10, 20, and 30 min of DUV+O_2 treatment, respectively. We note that the Dirac point was initially near ~0 V for pristine graphene on all substrates. The Dirac point shift of h-BN/graphene/h-BN was minute compared with that on other substrates. The Dirac point shift was only 7 V after 30 min of DUV+O_2 treatment. The h-BN/graphene/h-BN sandwich structure offers an advantage for manufacturing stable graphene electronic devices. The van der Waals interaction between the interfaces between graphene and h-BN may obstruct O_2 molecules from penetrating into the interface between graphene and h-BN,[48-50] whereas gas absorption has been generally observed in graphene on the conventional Si/SiO_2 substrate.

4. Conclusion

We reported uniform and high-quality graphene on CVD-grown h-BN substrate. In Raman spectroscopy, the FWHM and peak positions of graphene on different substrates revealed lower charge impurities for graphene on h-BN film. Electrical transport measurements revealed that graphene on h-BN film exhibited high mobility and restraint of charged impurities compared with graphene on SiO_2. The hole mobility of graphene on h-BN and h-BN/graphene/h-BN was 18000 and 20000 cm^2/Vs, respectively, at $T = 4.2$ K. Graphene enclosed by h-BN, i.e., h-BN/graphene/h-BN, showed the highest mobility for the entire temperature range in this experiment. The h-BN film provided not only an ideal substrate for graphene but also a protection layer preventing unwanted doping by O_2 gas. The h-BN/graphene/h-BN sandwich structure offered great advantage for the manufacture of stable graphene electronic devices. This work demonstrated the potential of large-area growth of h-BN and a simplified transfer method for graphene/h-BN film to reduce impurities in the interface, as required by graphene-based electronic devices.

Methods

Fabrication of h-BN. Ammonia borane (Sigma-Aldrich, 97% pure) was used as a precursor to make the h-BN film. It was thermally decomposed into hydrogen, aminoborane, and borazine at a temperature range from 80 to 120 °C. Aminoborane was trapped by the filter to remove it. The growth of h-BN film was performed on Cu foil (Alfa Aesar, 99.8% pure, 25 μm thick) using thermal CVD. The mechanically polished and electropolished Cu foil was annealed at 990 °C for 30 min with H_2 gas at a flow rate of 5 standard cubic centimeters per minute (sccm). After this cleaning process, h-BN was synthesized with borazine gas and hydrogen at 997 °C for 30 min. The furnace was cooled from 997 to 500 °C at a rate of ~35 °C/min.

Graphene Growth and Transfer. The graphene used in this study was grown on 25-μm-thick Cu foils from Alfa Aesar (99.8% pure) via thermal CVD. A mechanically polished and electropolished Cu foil was inserted into a thermal CVD furnace. The furnace was evacuated to $\sim 10^{-4}$ Torr, and the temperature increased to 1010 °C with H_2 gas flow ($\sim 10^{-2}$ Torr). After the temperature became stable at 1010 °C, both CH_4 (20 sccm) and H_2 (5 sccm) were injected into the furnace to synthesize the graphene for 8 min. After the graphene synthesis, the sample was cooled to room temperature at a rate of 50 °C/min. The typical grain size of graphene used in this work is about few tens of μm (30 – 70 μm). Graphene films were transferred onto Si/SiO_2 wafers as follows. Cu foil was etched in an aqueous solution of APS. The surface of the graphene was spin-coated with PMMA, and the sample was then baked at 70 °C for 10 min. The PMMA coating was applied to prevent the graphene film from cracking and folding during transfer to the desired substrate. PMMA/graphene film was washed with deionized water after the Cu foil had completely dissolved, and was then transferred onto the Si/SiO_2 wafer. The PMMA film was removed with organic solvent. The graphene sample was subsequently cleaned in isopropanol and dried in a N_2 flow. A simplified transfer method for graphene/h-BN film has been described in the Supporting Information.

Acknowledgment

This research was supported by the Basic Science Research Program (2010-0020207, 2013R1A1A2061396) through the NRF funded by the Ministry of Education and the Nanomaterial Technology Development Program (2012M3A7B4049888) through the National Research Foundation of Korea (NRF) funded by the Ministry of Science, ICT and Future Planning. We appreciate the efforts of Dr. June Park at the initial stage of this work.

Figure captions

Figure 1. (a) Schematic diagram of the h-BN growth process by using thermal CVD; (b) and (c) SEM images of growth morphology of CVD h-BN on Cu foil. (d) Optical image of the graphene device used in our study in which one part of the CVD-grown graphene is transferred to the Si/SiO$_2$ substrate while another is on CVD-grown h-BN film. The scale bar is 50 µm. (e) Raman spectra of CVD-grown h-BN transferred onto Si/SiO$_2$ substrate. The h-BN peak was observed at 1369 cm^{-1}, confirming the growth and clean transfer of h-BN onto Si/SiO$_2$ from Cu foil.

Figure 2. (a) Raman spectrum of CVD-grown graphene transferred onto a Si/SiO$_2$ substrate, h-BN film, and graphene sandwich between h-BN films. (b) The G peak was observed at 1584.4 and 1581.5 cm^{-1} on the SiO$_2$ and h-BN films, respectively. The G peak of h-BN/graphene/h-BN was observed at 1581.1 cm^{-1}. (c) The 2D peak was observed at 2684.1 and 2688.6 cm^{-1} on the SiO$_2$ and h-BN films, respectively. The FWHM of the 2D peak was 34.1 and 24.6 cm^{-1} on the SiO$_2$ and h-BN films, respectively. The 2D-peak position of the graphene sandwich between h-BN films was observed at 2694.2 cm^{-1} and was considerably blue-shifted by 10 cm^{-1} compared with the graphene on SiO$_2$. The FWHM of the 2D peak was 22.1 cm^{-1} for the graphene sandwich between h-BN films.

Figure 3. (a) Statistical distribution of the G-peak position of graphene on SiO$_2$, h-BN, and between h-BN films. The mean value of the distribution on h-BN was 1581.9 cm^{-1}, which is red-shifted with respect to the one on SiO$_2$, i.e., 1584.9 cm^{-1}. (b) Statistical distribution of the 2D-peak position of graphene on SiO$_2$, h-BN, and between the h-BN films. The mean value of the distribution on h-BN was 2688.1 cm^{-1}, which is blue-shifted with

respect to the one on SiO_2, i.e., 2684.5 cm^{-1}. (c) Statistical distribution of the Raman intensity ratio of I_{2D}/I_G for graphene/SiO_2, graphene/h-BN, and h-BN/graphene/h-BN. The mean value of I_{2D}/I_G was 2.5 for graphene on SiO_2, 5 for graphene on h-BN, and 6.8 for h-BN/graphene/h-BN. (d) The mean FWHM was 33.9 cm^{-1} for graphene/SiO_2, 24.8 cm^{-1} for graphene/h-BN, and 22.1 cm^{-1} for h-BN/graphene/h-BN.

Figure 4. (a) Back-gate-voltage (V_{bg})-dependent resistivity for CVD-grown graphene on h-BN film at different temperatures. The inset shows an optical micrograph of a graphene Hall bar structure for transport measurement. (b) Longitudinal resistivity (black curve) and the Hall conductance (red curve) as a function of V_{bg} at the magnetic field B = 9 T and temperature T = 0.33 K. (c) Hall plateau at the filling factor $\nu = \pm 1$ at a high magnetic field of 9 T. (d) Comparison of hole mobility among graphene devices on different substrates. The hole mobility of graphene on SiO_2, h-BN, and h-BN/graphene/h-BN was 2800, 6300, and 7400 cm^2/Vs, respectively, at T = 300 K, and 4000, 18000, and 20000 cm^2/Vs, respectively, at T = 4.2 K.

Figure 5. Back-gate-voltage (V_{bg})-dependent resistivity of the graphene devices after different DUV exposure times in O_2 gas flow (DUV+O_2); (a) on SiO_2; (b) on h-BN; (c) in the h-BN/G/h-BN device. (d) Dirac point shifts after 5, 10, 20, and 30 min of DUV illumination on different substrates. The Dirac point of graphene on SiO_2 film was observed at 21, 28, 32, and 36 V after 5, 10, 20, and 30 min of DUV+O_2 treatment, respectively, and on the h-BN film at 9.4, 12.7, 15, and 20 V after 5, 10, 20, and 30 min of DUV+O_2 treatment, respectively. The Dirac point was initially near ~0 V for pristine graphene on all substrates. The Dirac point shift of h-BN/graphene/h-BN is 7 V after 30 min of DUV+O_2 treatment.

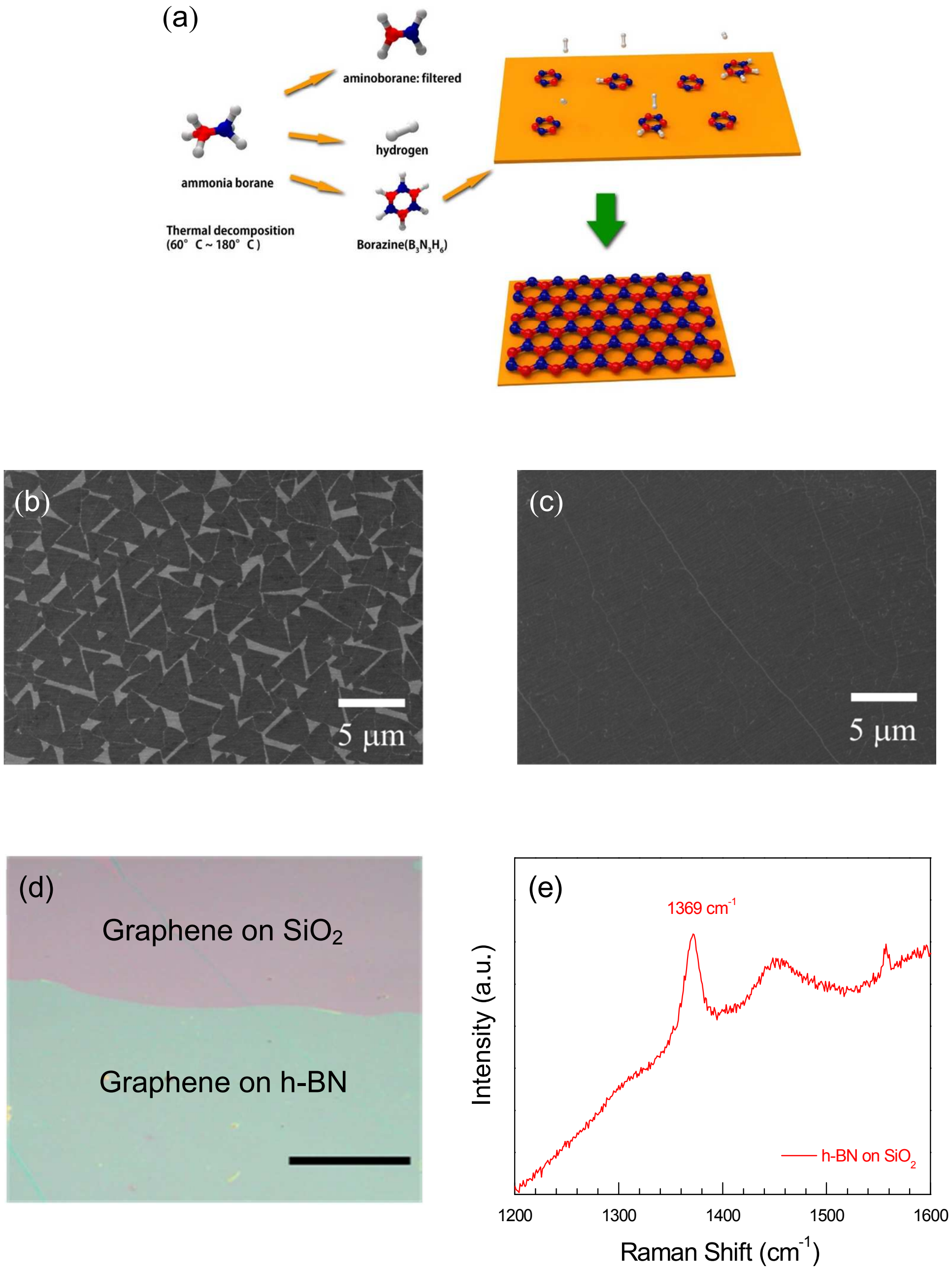
(a)
aminoborane: filtered
hydrogen
ammonia borane
Borazine($B_3N_3H_6$)
Thermal decomposition
(60° C ~ 180° C)
(b)
5 μm
(c)
5 μm
(d)
Graphene on SiO_2
Graphene on h-BN
(e)
1369 cm^{-1}
h-BN on SiO_2
Intensity (a.u.)
Raman Shift (cm^{-1})
1200
1300
1400
1500
1600

Figure 1

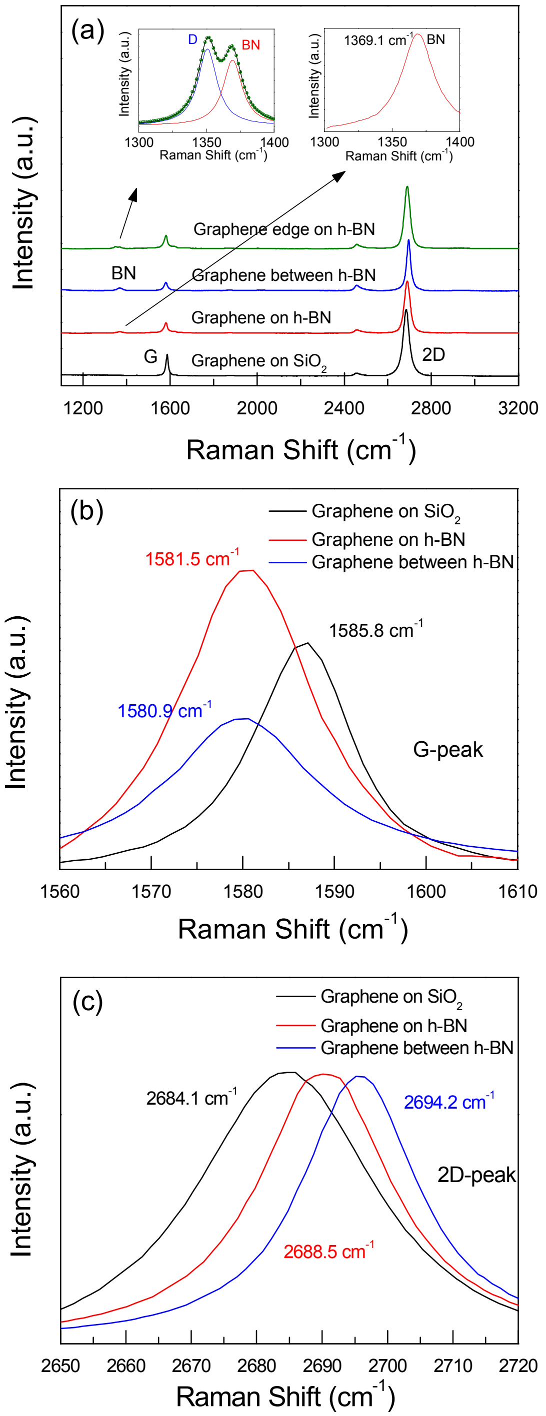
(a)
Intensity (a.u.)
D
BN
1300
1350
1400
Raman Shift (cm^{-1})
1369.1 cm^{-1}
BN
Graphene edge on h-BN
BN
Graphene between h-BN
Graphene on h-BN
G
Graphene on SiO$_2$
2D
1200
1600
2000
2400
2800
3200
Raman Shift (cm^{-1})
(b)
Graphene on SiO$_2$
Graphene on h-BN
Graphene between h-BN
1581.5 cm^{-1}
1585.8 cm^{-1}
1580.9 cm^{-1}
G-peak
Intensity (a.u.)
1560
1570
1580
1590
1600
1610
Raman Shift (cm^{-1})
(c)
Graphene on SiO$_2$
Graphene on h-BN
Graphene between h-BN
2684.1 cm^{-1}
2694.2 cm^{-1}
2D-peak
2688.5 cm^{-1}
Intensity (a.u.)
2650
2660
2670
2680
2690
2700
2710
2720
Raman Shift (cm^{-1})

Figure 2

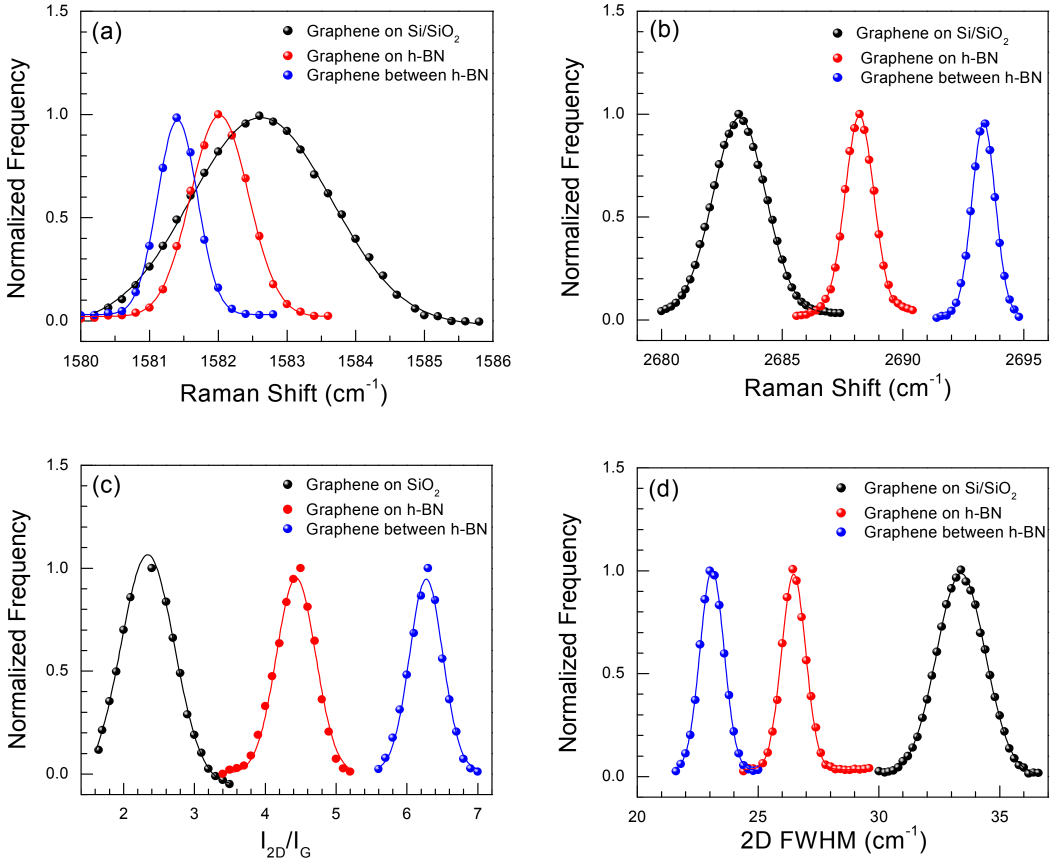
(a)
● Graphene on Si/SiO$_2$
● Graphene on h-BN
● Graphene between h-BN
Normalized Frequency
Raman Shift (cm^{-1})
1580 1581 1582 1583 1584 1585 1586
0.0 0.5 1.0 1.5
(b)
● Graphene on Si/SiO$_2$
● Graphene on h-BN
● Graphene between h-BN
Normalized Frequency
Raman Shift (cm^{-1})
2680 2685 2690 2695
0.0 0.5 1.0 1.5
(c)
● Graphene on SiO$_2$
● Graphene on h-BN
● Graphene between h-BN
Normalized Frequency
I$_{2D}$/I$_G$
2 3 4 5 6 7
0.0 0.5 1.0 1.5
(d)
● Graphene on Si/SiO$_2$
● Graphene on h-BN
● Graphene between h-BN
Normalized Frequency
2D FWHM (cm^{-1})
20 25 30 35
0.0 0.5 1.0 1.5

Figure 3

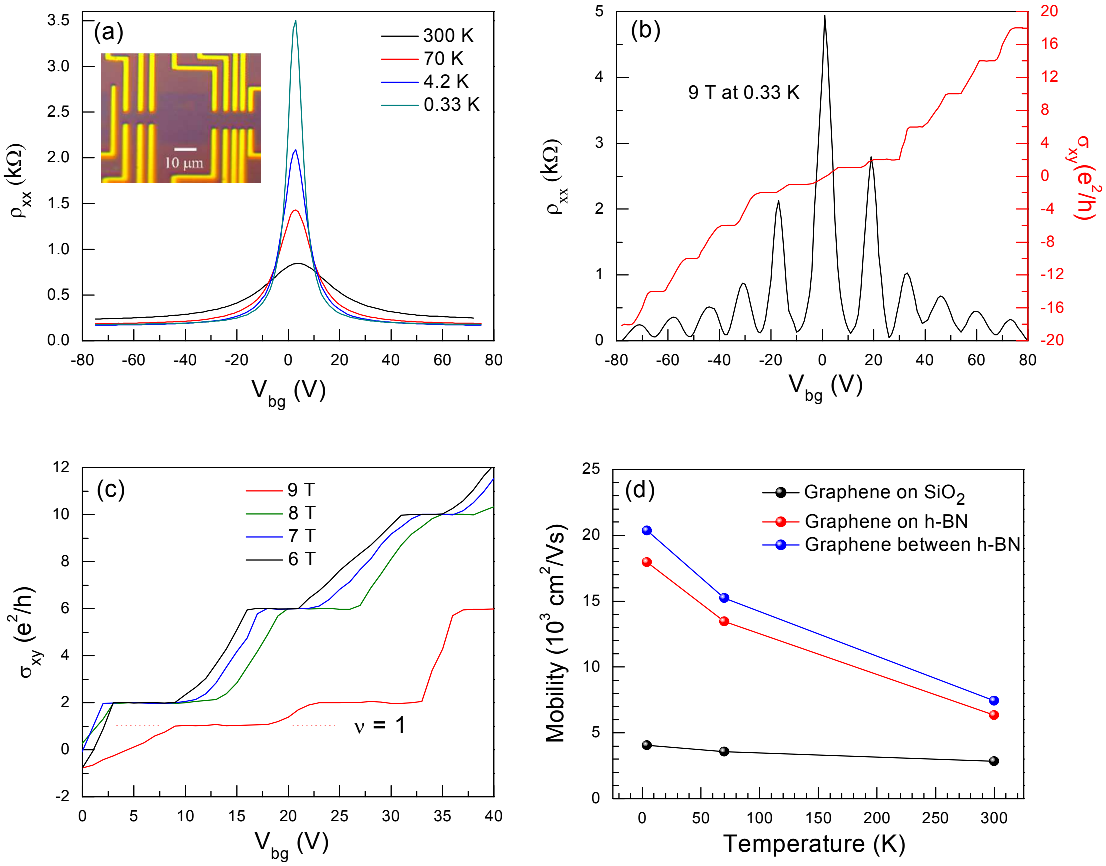
(a)
300 K
70 K
4.2 K
0.33 K
10 μm
ρxx (kΩ)
Vbg (V)
(b)
9 T at 0.33 K
ρxx (kΩ)
σxy (e²/h)
Vbg (V)
(c)
9 T
8 T
7 T
6 T
ν = 1
σxy (e²/h)
Vbg (V)
(d)
Graphene on SiO2
Graphene on h-BN
Graphene between h-BN
Mobility (10³ cm²/Vs)
Temperature (K)

Figure 4

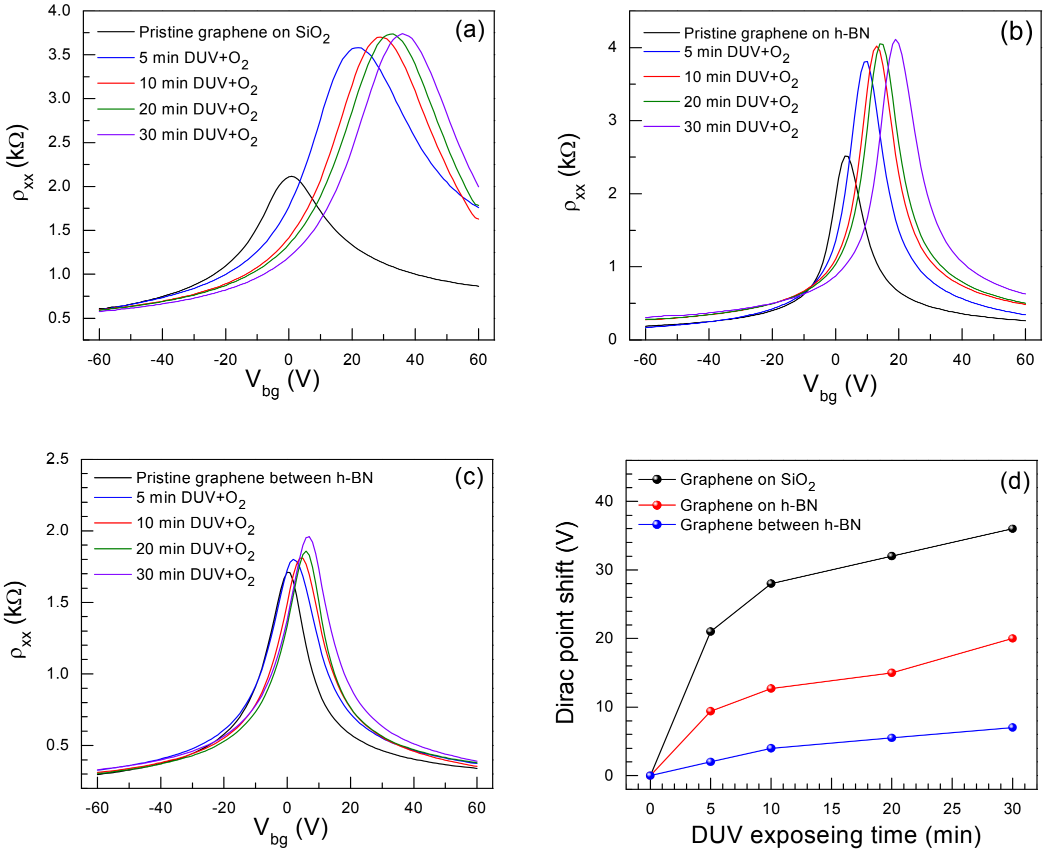
(a)
Pristine graphene on SiO$_2$
5 min DUV+O$_2$
10 min DUV+O$_2$
20 min DUV+O$_2$
30 min DUV+O$_2$
ρ_{xx} (kΩ)
4.0
3.5
3.0
2.5
2.0
1.5
1.0
0.5
-60
-40
-20
0
20
40
60
V_{bg} (V)
(b)
Pristine graphene on h-BN
5 min DUV+O$_2$
10 min DUV+O$_2$
20 min DUV+O$_2$
30 min DUV+O$_2$
ρ_{xx} (kΩ)
4
3
2
1
0
-60
-40
-20
0
20
40
60
V_{bg} (V)
(c)
Pristine graphene between h-BN
5 min DUV+O$_2$
10 min DUV+O$_2$
20 min DUV+O$_2$
30 min DUV+O$_2$
ρ_{xx} (kΩ)
2.5
2.0
1.5
1.0
0.5
-60
-40
-20
0
20
40
60
V_{bg} (V)
(d)
Graphene on SiO$_2$
Graphene on h-BN
Graphene between h-BN
Dirac point shift (V)
40
30
20
10
0
0
5
10
15
20
25
30
DUV exposeing time (min)

Figure 5

References

1. A. Pirkle, J. Chan, A. Venugopal, D. Hinojos, C. Magnuson, S. McDonnell, L. Colombo, E. Vogel, R. Ruoff and R. Wallace, *Applied Physics Letters*, 2011, 99, 122108.
2. Q. H. Wang, Z. Jin, K. K. Kim, A. J. Hilmer, G. L. Paulus, C.-J. Shih, M.-H. Ham, J. D. Sanchez-Yamagishi, K. Watanabe and T. Taniguchi, *Nature chemistry*, 2012, 4, 724-732.
3. E. Hwang and S. D. Sarma, *Physical Review B*, 2008, 77, 115449.
4. K. I. Bolotin, K. J. Sikes, Z. Jiang, M. Klima, G. Fudenberg, J. Hone, P. Kim and H. L. Stormer, *Solid State Commun*, 2008, 146, 351-355.
5. S. Berciaud, S. Ryu, L. E. Brus and T. F. Heinz, *Nano Lett*, 2009, 9, 346-352.
6. E. V. Castro, H. Ochoa, M. I. Katsnelson, R. V. Gorbachev, D. C. Elias, K. S. Novoselov, A. K. Geim and F. Guinea, *Phys Rev Lett*, 2010, 105, 266601.
7. M. M. Fogler, F. Guinea and M. I. Katsnelson, *Phys Rev Lett*, 2008, 101,226804.
8. S. Adam and S. Das Sarma, *Solid State Commun*, 2008, 146, 356-360.
9. M. P. Levendorf, C. J. Kim, L. Brown, P. Y. Huang, R. W. Havener, D. A. Muller and J. Park, *Nature*, 2012, 488, 627-632.
10. L. Ci, L. Song, C. H. Jin, D. Jariwala, D. X. Wu, Y. J. Li, A. Srivastava, Z. F. Wang, K. Storr, L. Balicas, F. Liu and P. M. Ajayan, *Nat Mater*, 2010, 9, 430-435.
11. C. R. Dean, A. F. Young, I. Meric, C. Lee, L. Wang, S. Sorgenfrei, K. Watanabe, T. Taniguchi, P. Kim, K. L. Shepard and J. Hone, *Nat Nanotechnol*, 2010, 5, 722-726.

12. Z. Liu, L. L. Ma, G. Shi, W. Zhou, Y. J. Gong, S. D. Lei, X. B. Yang, J. N. Zhang, J. J. Yu, K. P. Hackenberg, A. Babakhani, J. C. Idrobo, R. Vajtai, J. Lou and P. M. Ajayan, *Nat Nanotechnol*, 2013, 8, 119-124.

13. L. Liu, Y. P. Feng and Z. X. Shen, *Physical Review B*, 2003, 68,104102.

14. K. Watanabe, T. Taniguchi and H. Kanda, *Nat Mater*, 2004, 3, 404-409.

15. C. Y. Zhi, Y. Bando, C. C. Tang, H. Kuwahara and D. Golberg, *Adv Mater*, 2009, 21, 2889-93.

16. C. Ronning, E. Dreher, H. Feldermann, M. Gross, M. Sebastian and H. Hofsass, *Diam Relat Mater*, 1997, 6, 1129-1134.

17. T. Sugino, T. Tai and Y. Etou, *Diam Relat Mater*, 2001, 10, 1375-1379.

18. W. Gannett, W. Regan, K. Watanabe, T. Taniguchi, M. F. Crommie and A. Zettl, *Applied Physics Letters*, 2011, 98, 242105.

19. H. Wang, T. Taychatanapat, A. Hsu, K. Watanabe, T. Taniguchi, P. Jarillo-Herrero and T. Palacios, *Ieee Electr Device L*, 2011, 32, 1209-1211.

20. X. L. Li, X. P. Hao, M. W. Zhao, Y. Z. Wu, J. X. Yang, Y. P. Tian and G. D. Qian, *Adv Mater*, 2013, 25, 2200-2204.

21. L. Wang, I. Meric, P. Y. Huang, Q. Gao, Y. Gao, H. Tran, T. Taniguchi, K. Watanabe, L. M. Campos, D. A. Muller, J. Guo, P. Kim, J. Hone, K. L. Shepard and C. R. Dean, *Science*, 2013, 342, 614-617.

22. K. H. Lee, H. J. Shin, J. Lee, I. Y. Lee, G. H. Kim, J. Y. Choi and S. W. Kim, *Nano Lett*, 2012, 12,

714-718.

23. L. Song, L. J. Ci, H. Lu, P. B. Sorokin, C. H. Jin, J. Ni, A. G. Kvashnin, D. G. Kvashnin, J. Lou, B. I. Yakobson and P. M. Ajayan, *Nano Lett*, 2010, 10, 3209-3215.

24. K. K. Kim, A. Hsu, X. T. Jia, S. M. Kim, Y. M. Shi, M. Dresselhaus, T. Palacios and J. Kong, *Acs Nano*, 2012, 6, 8583-8590.

25. M. Her, R. Beams and L. Novotny, *Phys Lett A*, 2013, 377, 1455-1458.

26. W. Yang, G. R. Chen, Z. W. Shi, C. C. Liu, L. C. Zhang, G. B. Xie, M. Cheng, D. M. Wang, R. Yang, D. X. Shi, K. Watanabe, T. Taniguchi, Y. G. Yao, Y. B. Zhang and G. Y. Zhang, *Nat Mater*, 2013, 12, 792-797.

27. M. Wang, S. K. Jang, W. J. Jang, M. Kim, S. Y. Park, S. W. Kim, S. J. Kahng, J. Y. Choi, R. S. Ruoff, Y. J. Song and S. Lee, *Adv Mater*, 2013, 25, 2746-2752.

28. S. Tang, H. Wang, Y. Zhang, A. Li, H. Xie, X. Liu, L. Liu, T. Li, F. Huang and X. Xie, *Scientific reports*, 2013, 3,2666.

29. M. W. Iqbal, M. Z. Iqbal, X. Jin, C. Hwang and J. Eom, *ACS applied materials & interfaces*, 2014, 6, 4207-4213.

30. P. J. Zomer, S. P. Dash, N. Tombros and B. J. van Wees, *Applied Physics Letters*, 2011, 99, 232104.

31. R. Geick, C. H. Perry and Rupprech.G, *Phys Rev*, 1966, 146, 543-547.

32. A. C. Ferrari, *Solid State Commun*, 2007, 143, 47-57.

33. C. Casiraghi, A. Hartschuh, H. Qian, S. Piscanec, C. Georgi, A. Fasoli, K. S. Novoselov, D. M. Basko and A. C. Ferrari, *Nano Lett*, 2009, 9, 1433-1441.

34. A. C. Ferrari, J. C. Meyer, V. Scardaci, C. Casiraghi, M. Lazzeri, F. Mauri, S. Piscanec, D. Jiang, K. S. Novoselov, S. Roth and A. K. Geim, *Phys Rev Lett*, 2006, 97, 187401.

35. D. C. Elias, R. R. Nair, T. M. G. Mohiuddin, S. V. Morozov, P. Blake, M. P. Halsall, A. C. Ferrari, D. W. Boukhvalov, M. I. Katsnelson, A. K. Geim and K. S. Novoselov, *Science*, 2009, 323, 610-613.

36. M. W. Iqbal, A. K. Singh, M. Z. Iqbal and J. Eom, *J Phys-Condens Mat*, 2012, 24,335301.

37. Z. H. Ni, T. Yu, Z. Q. Luo, Y. Y. Wang, L. Liu, C. P. Wong, J. M. Miao, W. Huang and Z. X. Shen, *Acs Nano*, 2009, 3, 569-574.

38. A. Das, S. Pisana, B. Chakraborty, S. Piscanec, S. K. Saha, U. V. Waghmare, K. S. Novoselov, H. R. Krishnamurthy, A. K. Geim, A. C. Ferrari and A. K. Sood, *Nat Nanotechnol*, 2008, 3, 210-215.

39. J. H. Chen, W. G. Cullen, C. Jang, M. S. Fuhrer and E. D. Williams, *Phys Rev Lett*, 2009, 102,236805.

40. S. Berciaud, X. L. Li, H. Htoon, L. E. Brus, S. K. Doorn and T. F. Heinz, *Nano Lett*, 2013, 13, 3517-3523.

41. D. M. Basko, *Physical Review B*, 2008, 78,125418.

42. Y. B. Zhang, Y. W. Tan, H. L. Stormer and P. Kim, *Nature*, 2005, 438, 201-204.

43. K. S. Novoselov, E. McCann, S. V. Morozov, V. I. Fal'ko, M. I. Katsnelson, U. Zeitler, D. Jiang, F. Schedin and A. K. Geim, *Nat Phys*, 2006, 2, 177-180.

44. K. S. Novoselov, Z. Jiang, Y. Zhang, S. V. Morozov, H. L. Stormer, U. Zeitler, J. C. Maan, G. S. Boebinger, P. Kim and A. K. Geim, *Science*, 2007, 315, 1379-1379.

45. J. Choi, H. Kim, J. Park, M. W. Iqbal, M. Z. Iqbal, J. Eom and J. Jung, *Current Applied Physics*, 2014, DOI: 10.1016/j.cap.2014.05.002.

46. M. Iqbal, M. F. Khan, M. W. Iqbal and J. Eom, *J Mater Chem C*, 2014,2,5404-5410.

47. M. Z. Iqbal, S. Siddique, M. W. Iqbal and J. Eom, *J Mater Chem C*, 2013, 1, 3078-3083.

48. L. Wang, Z. Y. Chen, C. R. Dean, T. Taniguchi, K. Watanabe, L. E. Brus and J. Hone, *Acs Nano*, 2012, 6, 9314-9319.

49. N. Marom, J. Bernstein, J. Garel, A. Tkatchenko, E. Joselevich, L. Kronik and O. Hod, *Phys Rev Lett*, 2010, 105,046801.

50. G. H. Gao, W. Gao, E. Cannuccia, J. Taha-Tijerina, L. Balicas, A. Mathkar, T. N. Narayanan, Z. Liu, B. K. Gupta, J. Peng, Y. S. Yin, A. Rubio and P. M. Ajayan, *Nano Lett*, 2012, 12, 3518-3525.